



Supplement of

A set of methods to evaluate the below-cloud evaporation effect on local precipitation isotopic composition: a case study for Xi'an, China

Meng Xing et al.

Correspondence to: Meng Xing (xingmeng@ieecas.cn) and Weiguo Liu (liuwg@loess.llqg.ac.cn)

The copyright of individual parts of the supplement might differ from the article licence.

Text S1: Isotopic composition-humidity dependency correction

Because we did not have the Standards Delivery Module (Picarro) system or equivalent, the isotopic composition-humidity correction is based on data obtained from discrete injections of three known liquid standards with a PAL autosampler and the Picarro vaporizer unit (Benetti et al., 2014; Noone et al., 2013). The analyzer is programmed to perform a self-calibration after every 24 hours of ambient air measurement using an autosampler to inject liquid standards for producing different humidity. Each reference sample is measured continuously for 8 times at one humidity level. To eliminate the memory effect, the first five injections were discarded, while the last three of eight injections were used to calculate the average δ -value at the measured humidity.

As reported by Weng et al. (2020), there are both isotope composition and humidity effects in our study, and thus we adopted Weng's et al. (2020) method to correct our data. There are six steps in the isotopic composition-humidity correction framework:

1. To obtain the humidity dependency for each water standard as raw (uncorrected) measurements of the isotope composition, we measured our three lab standards at the humidity range from 3000 to 30000 ppmv, as shown in Fig. S1a, and Fig. S1b.

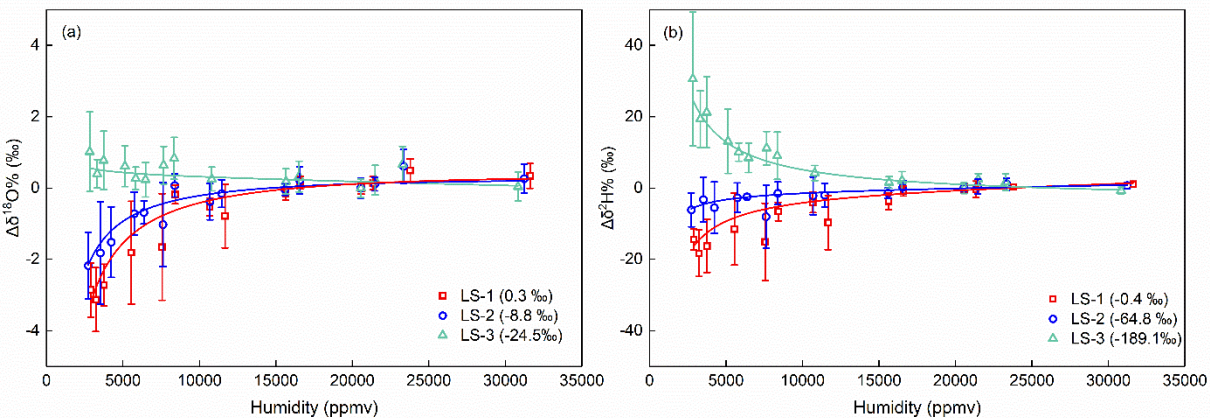


Figure S1. The isotopic composition-humidity correction for water vapor $\delta^{18}\text{O}_v$ (a); the same as (a), but for water vapor $\delta^2\text{H}_v$ (b); LS-1, LS-2, and LS-3 are three lab standards.

2. According to Eq. (S1), the humidity dependency for each water standard as the deviation of the raw measurements to the reference value at 20000 ppmv can be got. These deviations are denoted as $\Delta\delta^{18}\text{O}$ and $\Delta\delta^2\text{H}$.

$$\Delta\delta = \delta_{\text{meas}} - \delta_{\text{cor}} \quad (\text{S1})$$

3. Referring to Weng et al. (2020), we used the following fitting functions to fit the humidity dependency of each standard water:

$$f_{\delta}(x) = \frac{a_{\delta}}{x} + b_{\delta}x + c_{\delta} \quad (\text{S2})$$

where x is the humidity, δ indicates the isotope composition of the standard waters, and a_{δ} , b_{δ} , and c_{δ} are fitting coefficients for each water standard and isotope species.

According to Fig. S1a, and Fig. S1b, the fitting coefficients of a_{δ} , b_{δ} , and c_{δ} are summarized in Table S1.

Table S1. Fitting coefficients for the humidity dependency behavior of the three standard waters. Coefficients a , b , and c are calculated with respect to the fitting function Eq. (S2). The reported uncertainty is 1 standard deviation. The fitting lines are shown in Fig. S1

	Standard	a	b	c
$\delta^{18}\text{O}$	LS-1	-11520±2065	-5.05×10 ⁻⁶ ±1.70×10 ⁻⁵	0.79±0.42
	LS-2	-7386±1783	-4.23×10 ⁻⁶ ±1.38×10 ⁻⁵	0.57±0.35
	LS-3	658±1342	-1.02×10 ⁻⁵ ±1.34×10 ⁻⁵	0.36±0.33
$\delta^2\text{H}$	LS-1	-46183±7604	1.10×10 ⁻⁴ ±5.40×10 ⁻⁵	-0.58±1.61
	LS-2	-14531±5197	6.24×10 ⁻⁵ ±3.19×10 ⁻⁵	-0.61±1.00
	LS-3	76474±11901	-2.40×10 ⁻⁵ ±6.14×10 ⁻⁵	-2.22±1.98

4. The obtained fitting coefficients are expressed as a function of the isotope composition as $a(\delta)$, $b(\delta)$, and $c(\delta)$ for all the standard waters (Fig. S2). This reveals a dependency of the fitting coefficients on the isotope composition of the water standard.

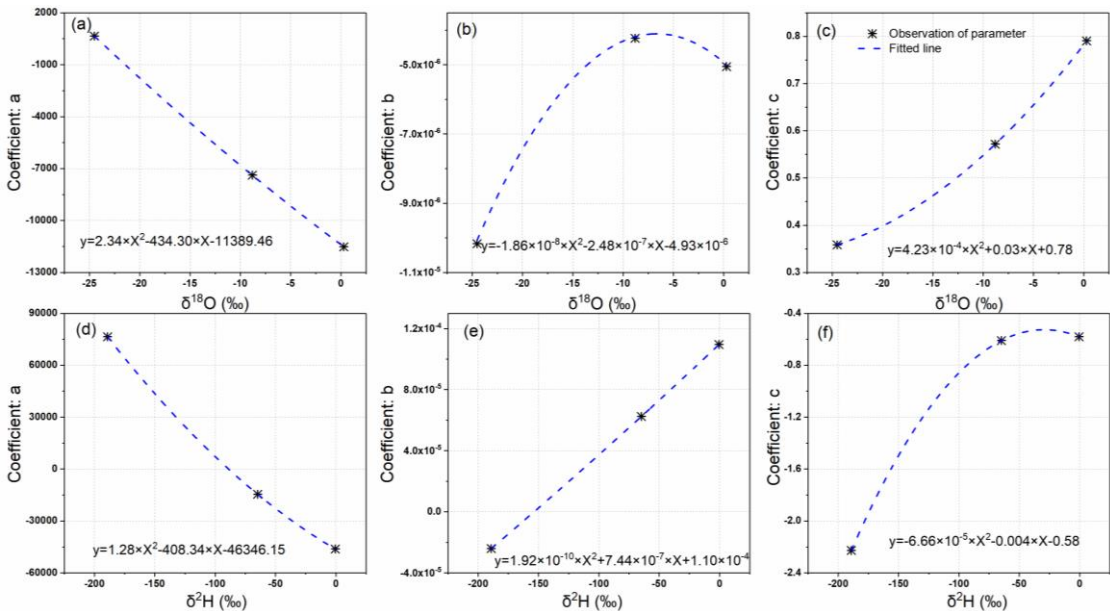


Figure S2. Dependency of fitting coefficients a , b , and c on $\delta^{18}\text{O}$ (a–c) and on $\delta^2\text{H}$ (d–f).

We now fit a suitable function to this dependency by using the following quadratic polynomial:

$$\left\{ \begin{array}{l} a(\delta) = m_a \times \delta^2 + n_a \times \delta + k_a \\ b(\delta) = m_b \times \delta^2 + n_b \times \delta + k_b \\ c(\delta) = m_c \times \delta^2 + n_c \times \delta + k_c \end{array} \right. \quad (S3)$$

where δ is the isotope composition and m , n , and k are the respective fitting coefficients of the quadratic polynomials. The coefficients m , n , and k are listed in Table S2.

Table S2. Coefficients m , n , and k are with respect to the fitting function Eq. (S3).

	Coefficient	m	n	k
$\delta^{18}\text{O}$	a	2.34	-434.30	-11389.46
	b	-1.86×10^{-8}	-2.48×10^{-7}	-4.93×10^{-6}
	c	4.23×10^{-4}	0.03	0.78
$\delta^2\text{H}$	a	1.28	-408.34	-46346.15
	b	1.92×10^{-10}	7.44×10^{-7}	1.10×10^{-4}
	c	-6.66×10^{-5}	-0.004	-0.58

5. By replacing the parameters a_δ , b_δ , and c_δ in Eq. (S2) with their parametric expressions in Eq. (S3), the generalized fitting for the mixing ratio dependency is obtained, which is a function of both the humidity x and the isotope composition of the measured water vapor δ as follows:

$$f_\delta(x, \delta) = \frac{a(\delta)}{x} + b(\delta)x + c(\delta) \quad (S4)$$

6. Using Eq. (S4), the measured water vapor isotope compositions to a reference humidity at 20000 ppmv can be corrected, when given any measured raw humidity and isotope composition within the range investigated here. Thus, the isotope composition at 20000 ppmv ($\delta_{\text{iso-hum-cor}}$) is the unknown; its analytical solution is found by solving the following equation:

$$\delta_{\text{meas}} - \delta_{\text{iso-hum-cor}} = \frac{a(\delta_{\text{iso-hum-cor}})}{h} + b(\delta_{\text{iso-hum-cor}})h + c(\delta_{\text{iso-hum-cor}}) \quad (S5)$$

where h is the measured raw humidity and δ_{meas} is the measured isotope composition at that humidity. The right-hand side of the equation is the isotopic deviation determined from Eq. (S4). The coefficients $a(\delta_{\text{iso-hum-cor}})$, $b(\delta_{\text{iso-hum-cor}})$, and $c(\delta_{\text{iso-hum-cor}})$ are determined from Eq. (S3). For the detailed procedure to obtain its analytical solution, please refer to Weng et al. (2020).

Text S2: $\Delta d\Delta\delta$ -diagram calculation

To calculate the precipitation equilibrated water vapor isotopic composition, we

hypothesize the constant exchange of water molecules between the liquid and the vapor phases during the falling of raindrops, and the isotopic compositions reach towards equilibrium in the two phases during the processes. In the equilibrium state, the isotopic fractionation between the liquid and vapor phases follows a temperature-dependent factor:

$$\alpha = \frac{R_{pv-eq}}{R_p} \quad (S6)$$

where R_{pv-eq} is the water vapor isotope ratio between heavy and light isotopes ($^2\text{H}/^1\text{H}$ and $^{18}\text{O}/^{16}\text{O}$), R_p is the isotope ratio in precipitation, and α is a temperature-dependent equilibrium fractionation factor. Here, when the temperature is greater than 0 °C, we use the equation of Horita and Wesolowski (1994) to calculate ${}^2\alpha$ and ${}^{18}\alpha$, when the temperature is below 0 °C, the equilibrium fractionation factor proposed by Ellehoj et al. (2013) is used.

The above equation can be converted into δ-notation as:

$$\delta_{pv-eq} = \frac{1}{\alpha} (\delta_p + 1000) - 1000 \quad (S7)$$

where δ_p is the isotope ratio in precipitation.

Text S3: Method 1 calculation

In Stewart's model (1975), the parameters of γ and β are defined as:

$$\gamma = \frac{\alpha h}{1 - \alpha (D/D')^k (1-h)} \quad (S8)$$

$$\beta = \frac{1 - \alpha (D/D')^k (1-h)}{\alpha (D/D')^k (1-h)} \quad (S9)$$

where α are equilibrium fractionation factors for hydrogen and oxygen isotopes, respectively (Ellehoj et al., 2013; Horita and Wesolowski, 1994); h is relative humidity; D/D' for ^2H and ^{18}O are 1.024 and 1.0289, respectively (Stewart, 1975; Wang et al., 2016); and k is 0.58.

According to the law of conservation of mass, the remaining fraction of raindrop mass can be calculated as:

$$F_r = \frac{m_{end}}{m_{end} + m_{ev}} \quad (S10)$$

where the mass of the reaching ground raindrop without evaporation is m_{end} and the evaporated raindrop mass is m_{ev} which is defined as:

$$m_{ev} = E t \quad (S11)$$

where E denotes the evaporation intensity (the loss of water mass per unit time) and t

stands for the falling time of a raindrop. The falling time of a raindrop is assumed to be only related to the height of the cloud base, expressed as Z, and to the terminal velocity of a raindrop, expressed as v_{end} , and the equation can be defined as:

$$t = \frac{Z}{v_{end}} \quad (S12)$$

According to Best (1950a) the terminal velocity of the raindrop is considered

$$v_{end} = \begin{cases} 9.58e^{0.0354Z} \left(1 - e^{-(D/1.77)^{1.147}}\right), & 0.3 \leq D < 6.0 \\ 1.88e^{0.0256Z} \left(1 - e^{-(D/0.304)^{1.819}}\right), & 0.05 \leq D < 0.3 \\ 28.40D^2 e^{0.0172Z}, & D < 0.05 \end{cases} \quad (S13)$$

where e is natural constant, Z is height at cloud base (km), and D is diameter of raindrop (mm).

The cloud-base height is determined as lifting condensation level (LCL) in this study and can be calculated using a barometric formula (von Herrmann, 1906):

$$Z = 18400 \left(1 + \frac{T_{mean}}{273}\right) \lg \frac{S_0}{S_{LCL}} \quad (S14)$$

where T_{mean} is the average air temperature ($^{\circ}\text{C}$) between LCL and surface, S_0 is measured pressure (hPa) at surface, and S_{LCL} is pressure (hPa) at LCL (Barnes, 1968) and is defined as

$$S_{LCL} = S_0 \left(\frac{T_{LCL}}{T_0}\right)^{3.5} \quad (S15)$$

where S_0 is pressure at the observation site (hPa) and T_{LCL} and T_0 are air temperature (K) at LCL and at the surface. Air temperature at LCL is calculated using an empirical formula (Barnes, 1968):

$$T_{LCL} = T_{dp} - (0.001296T_{dp} + 0.1963)(T_0 - T_{dp}) \quad (S16)$$

where T_{dp} and T_0 are the dewpoint and air temperature ($^{\circ}\text{C}$) at the observation sites.

The dew point temperature can be derived from observed temperature and relative humidity (Górnicki et al., 2017):

$$T_{dp} = \frac{237(\log_{10}h + \frac{7.5T_0}{237+T_0})}{7.5 - \log_{10}h - \frac{7.5T_0}{237+T_0}} \quad (S17)$$

The evaporation intensity of falling drops is determined by a matrix that is composed of Q1 and Q2 (Kinzer and Gunn, 1951):

$$E = Q1(T, D)Q2(T, h) \quad (S18)$$

where Q1 is part of the function (cm) which is related to the ambient air temperature and raindrop diameter, and Q2 part ($\text{g cm}^{-1} \text{ s}^{-1}$) is combination of air temperature and relative humidity. Following the results of Kinzer and Gunn (1951), the values of Q1 and Q2 for specific conditions are acquired by using a bilinear interpolation method which is suggested by Wang et al. (2016).

To estimate the raindrop diameter, an empirical formula suggested by Best (1950b) is applied:

$$1-F = e^{-(D/AI^q)^c} \quad (\text{S19})$$

where F is the fraction of raindrops with diameter less than D; I is precipitation intensity (mm h^{-1}) which can be calculated according to the precipitation amount and duration; c, A, and q are constants of 2.25, 1.30, and 0.232, respectively. Assuming F = 0.5, the median size of the raindrop is solved as:

$$D_{50} = \sqrt[6]{0.69AI^q} \quad (\text{S20})$$

Text S4: Method 2 calculation

The precipitation isotopic composition at the cloud base follows the equilibrium fractionation with the ambient water vapor, and is defined as:

$$R_{cb-p} = R_{cb-v}\alpha \quad (\text{S21})$$

and can be equivalently rewritten in δ -notation as:

$$\frac{\delta_{cb-p}}{1000} + 1 = \alpha \left(\frac{\delta_{cb-v}}{1000} + 1 \right)$$

In the case of the moist adiabatic ascent of an isolated air mass continuously losing condensate by the rainout process, the Rayleigh formula leads to the isotopic composition of the tropospheric water vapor as a function of altitude (Sonntag et al., 1983). Therefore, the water vapor isotopic composition at the cloud base that follows the vertical distribution of Rayleigh distillation can be described by the following equation (Araguás-Araguás et al., 2000; Deshpande et al., 2010):

$$\delta_{cb-v} = 1000 \left\{ (1 + 1000\delta_{gr-v}) \exp(-(\alpha-1)(Z/Z_0)) \right\} - 1000 \quad (\text{S22})$$

where α is the equilibrium fractionation factor at a temperature of the height of Z; δ_{gr-v} is observed water vapor isotopic composition at the ground level; Z is the height of the cloud base; and Z_0 denotes the scale height of the atmospheric water vapor distribution. The values of Z_0 in low latitudes are discussed by Parameswaran and Krishnamurthy (1990). The height of the cloud base can be calculated by using Eq. (S14), while the temperature at cloud base can be solved by Eq. (S16).

In turn, if the deviations of isotopic composition caused by below-cloud evaporation and the parameters (e.g. γ , β , and α) are determined, the evaporated part of raindrop mass can be calculated by:

$$F_r = \sqrt{\beta \frac{\Delta\delta_p}{(1-\alpha)} + 1} \quad (S23)$$

Text S5: Assessment of uncertainty

The uncertainty of calculating the below-cloud evaporation effect on precipitation isotopic compositions by the two methods can be derived by the equation as follows (Wu et al., 2022):

$$W = \sqrt{2 \left\{ \left[\frac{w_{\delta_1}}{(\delta_{lower} - \delta_{upper})} \right]^2 + \left[\frac{w_{\delta_2}}{(\delta_{lower} - \delta_{upper})} \right]^2 + \dots + \left[\frac{w_{\delta_n}}{(\delta_{lower} - \delta_{upper})} \right]^2 \right\}} \quad (S24)$$

Where δ_{lower} and δ_{upper} are the isotopic compositions of $\Delta\delta^2H_p$ at the observation site derived from the low and upper limits of input parameters, respectively, including the variation of temperature, RH, and precipitation amount in method 1, and temperature, RH, ground level water vapor δ^2H_{gr-v} , and precipitation δ^2H_p in method 2. We vary each of the input parameters one at a time over a range taking the lower and upper value from the adopted sources of the data. $w_{\delta n}$ with different terms represents the uncertainty of isotopic compositions in $\Delta\delta^2H_p$ in the variables specified in the subscript, caused by the various input parameters.

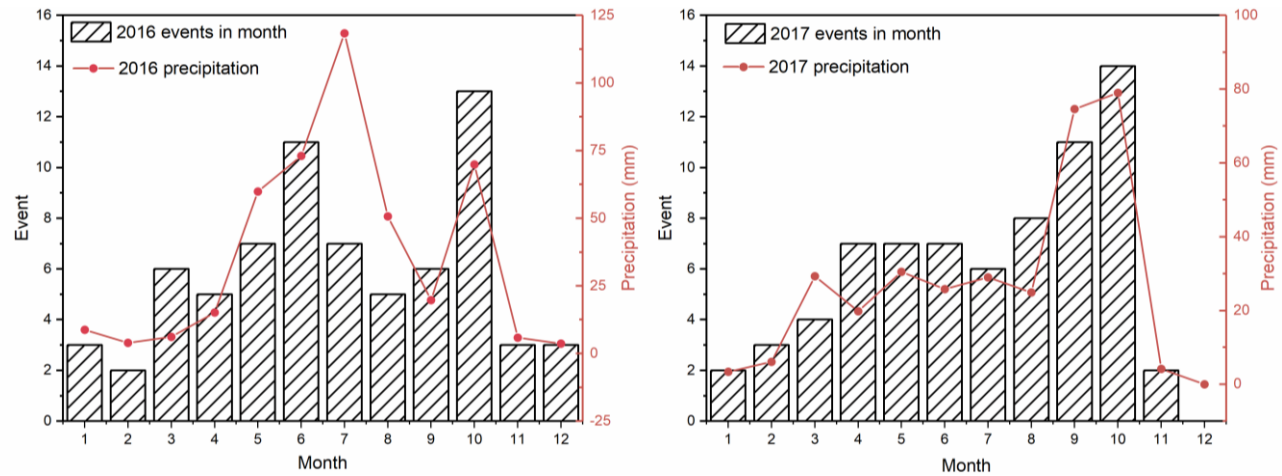


Figure S3. The distributions of the precipitation event and amount in the year

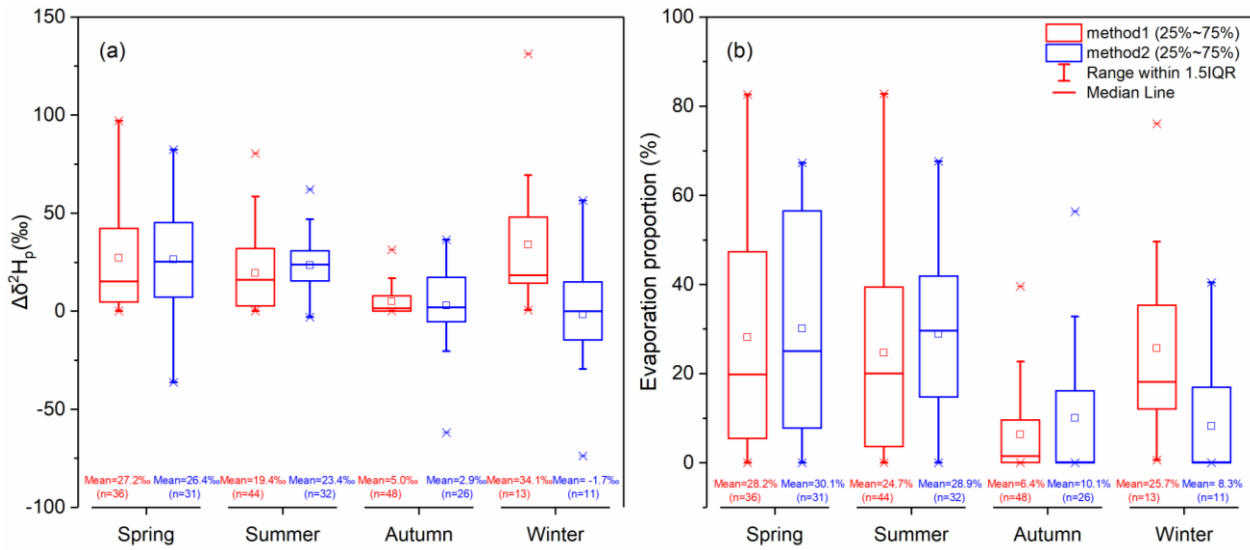


Figure S4. The seasonal variations in $\Delta\delta^2H_p$ in method 1 and method 2(a); the same as (a) but for the evaporation proportion (F_i) (b).

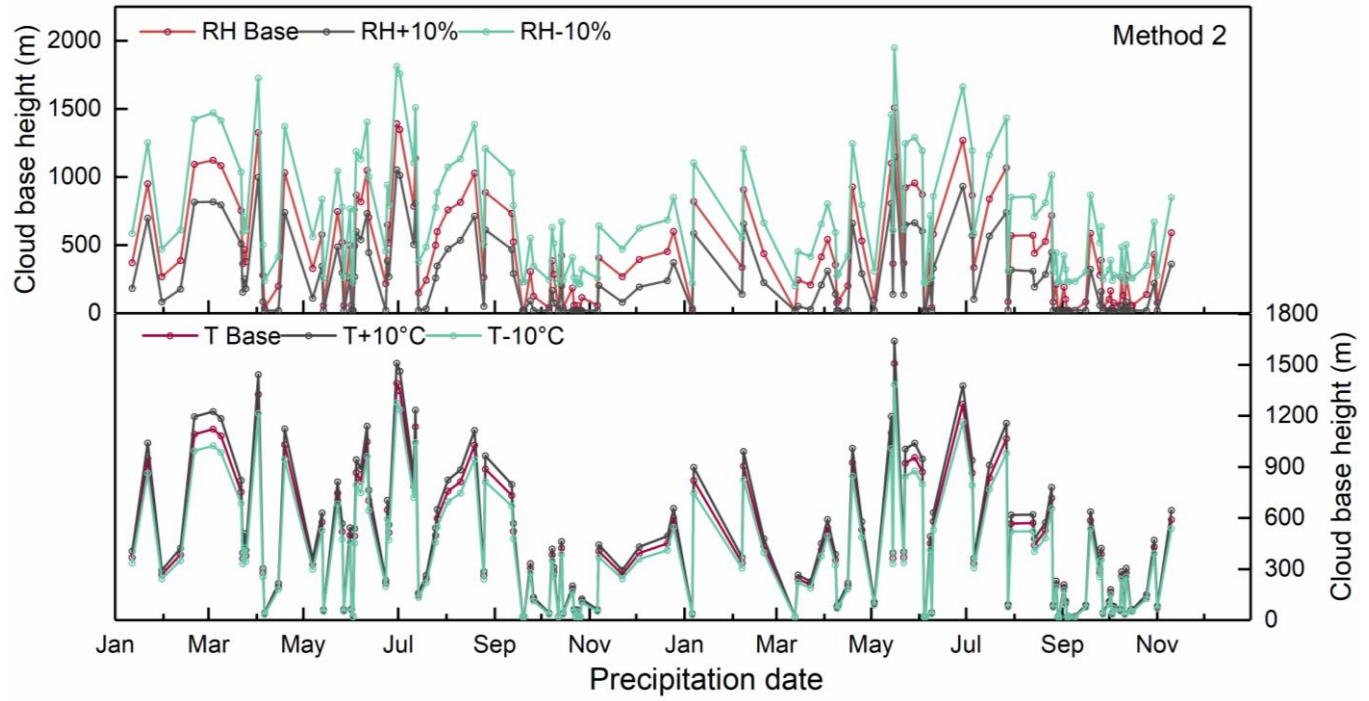


Figure S5. The effect of RH variations on the cloud base height (a); the same as (a) but for temperature effect.

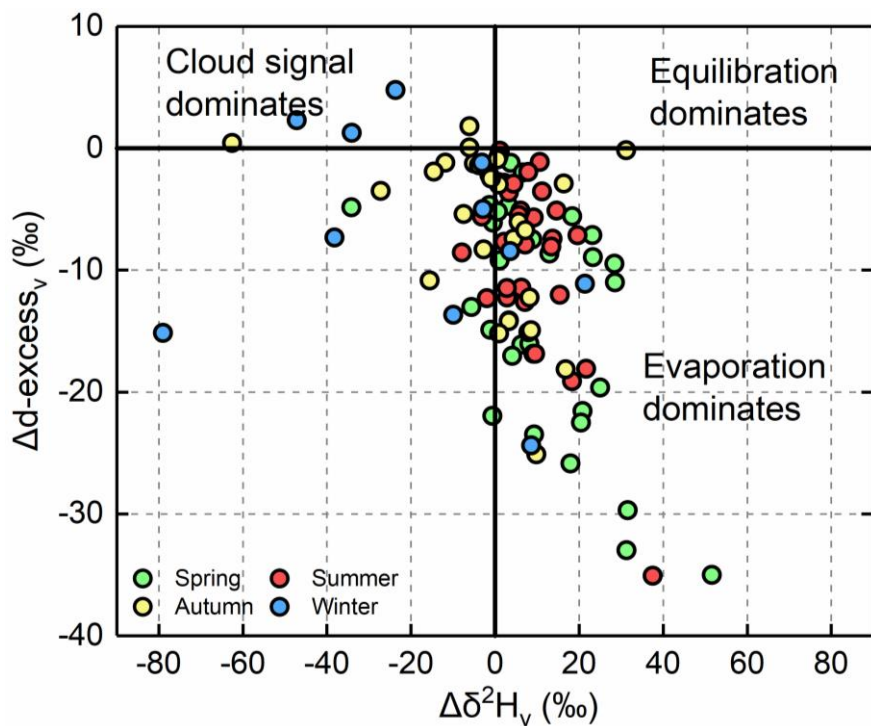


Figure S6. The projection of our data on $\Delta d\Delta\delta$ -diagram and separated by seasons.

Table S3. Summary of event-based meteorological, precipitation, and water vapor data used in this study

Date	Type	T °C	RH %	P mm	Duration h	$\delta^{18}\text{O}_p$ ‰	$\delta^2\text{H}_p$ ‰	d-excess _p ‰	$\delta^{18}\text{O}_v$ ‰	$\delta^2\text{H}_v$ ‰	d-excess _v ‰
2016-01-12	Snow	-0.1	80	1.3	13.0	-3.3	-32.4	-6.0	-21.7	-154.9	18.8
2016-01-22	Snow	-1.6	55	1.2	4.0	-15.8	-106.0	20.4	-26.6	-190.0	22.6
2016-01-31	Snow	-1.0	85	6.3	12.0	-8.7	-41.8	27.8	-18.6	-122.1	27.0
2016-02-12	Snow	4.5	80	3.8	9.0	-4.6	-20.1	16.7	-14.3	-89.2	25.5
2016-02-21	Snow	1.2	51	0.2	6.0	-10.1	-61.4	19.4	-17.9	-122.4	20.8
2016-03-04	Rain	10.4	53	1.4	4.0	8.8	61.2	-9.2	-12.7	-83.7	17.8
2016-03-09	Snow	3.3	52	0.6	7.0	0.6	18.3	13.5	-15.0	-94.2	25.4
2016-03-22	Rain	11.2	66	2.2	15.0	2.8	24.7	2.3	-13.3	-89.5	16.9
2016-03-23	Rain	10.5	82	0.8	21.0	-0.7	13.4	19.0	-11.9	-77.8	17.3
2016-03-24	Rain	8.3	77	0.1	5.0	1.2	8.6	-1.0	-15.4	-103.3	15.8
2016-03-25	Rain	8.5	81	1.1	4.0	-5.1	-32.5	8.3	-18.6	-125.9	22.9
2016-04-02	Rain	19.9	50	0.6	8.0	0.3	7.6	5.2	-13.5	-80.2	27.8
2016-04-05	Rain	11.0	86	3.6	7.0	0.8	12.2	5.8	-12.4	-75.5	23.6
2016-04-06	Rain	12.2	98	2.0	19.0	0.5	14.5	10.5	-12.4	-76.0	20.7
2016-04-15	Rain	12.7	90	8.3	12.0	-6.0	-35.5	12.5	-20.3	-141.1	21.4
2016-04-19	Rain	17.4	58	0.7	3.0	3.4	18.9	-8.5			
2016-05-07	Rain	13.3	84	6.1	19.0	1.6	24.0	11.5	-10.0	-63.9	16.1
2016-05-13	Rain	11.7	73	9.2	6.0	1.3	12.0	1.8	-12.2	-83.7	13.8
2016-05-14	Rain	10.7	97	28.2	19.0	-8.9	-55.5	15.6	-15.7	-104.0	21.4
2016-05-23	Rain	18.5	68	6.6	16.0	-2.3	-5.2	13.5			
2016-05-26	Rain	15.2	76	1.4	12.0	-4.2	-30.6	2.6	-15.4	-105.1	16.4
2016-05-27	Rain	14.0	97	4.9	21.0	-4.9	-26.6	12.2	-17.1	-117.2	19.7
2016-05-31	Rain	21.5	78	3.5	9.0	6.3	33.3	-17.4	-11.3	-76.8	14.0
2016-06-01	Rain	19.0	97	8.1	11.0	-0.1	3.5	4.1	-13.1	-84.7	20.3
2016-06-02	Rain	16.0	99	7.6	21.0	-3.0	-16.9	7.0	-14.9	-100.2	18.9
2016-06-03	Rain	20.4	78	0.4	1.0	-4.6	-23.1	13.4	-15.1	-102.0	18.5
2016-06-04	Rain	23.4	65	0.5	1.0	5.6	25.5	-19.3	-13.8	-88.4	14.9
2016-06-07	Rain	24.7	67	9.0	2.0	-4.8	-32.6	6.1	-17.5	-118.9	20.8
2016-06-11	Rain	26.5	60	8.5	4.0	-5.2	-23.6	17.7	-14.5	-94.7	21.0
2016-06-12	Rain	24.9	71	0.5	1.0	-2.6	-10.3	10.4	-14.5	-96.3	19.6
2016-06-23	Rain	22.7	90	33.2	15.0	-6.3	-37.3	13.3	-16.1	-110.4	18.6
2016-06-24	Rain	25.0	73	3.2	2.0	-5.5	-32.0	12.0	-16.6	-111.9	20.7
2016-06-25	Rain	25.3	78	0.5	1.0	-2.1	-17.9	-1.3	-13.8	-96.4	13.8
2016-06-30	Rain	28.8	51	1.6	0.5	-5.1	-36.2	4.3	-14.1	-95.3	17.4
2016-07-02	Rain	28.3	52	1.2	0.2	-2.2	-19.1	-1.5	-14.5	-97.3	18.5
2016-07-11	Rain	28.8	69	0.2	0.5	-8.5	-56.5	11.8	-18.9	-132.8	18.0
2016-07-12	Rain	28.8	58	0.5	2.0	-7.1	-50.3	6.4	-19.3	-136.0	18.7
2016-07-14	Rain	21.2	93	35.6	16.0	-8.6	-66.6	2.0	-19.4	-136.2	18.9
2016-07-19	Rain	24.2	89	8.9	14.0	-5.3	-51.3	-9.2			
2016-07-25	Rain	27.3	79	70.0	8.0	-9.3	-65.8	8.3			
2016-07-26	Rain	25.9	75	2.0	3.0	-6.2	-46.3	3.5	-16.6	-117.3	15.2
2016-08-02	Rain	29.2	70	3.1	0.5	-6.5	-42.8	9.0	-16.8	-115.1	18.9
2016-08-10	Rain	28.4	68	2.9	0.2	-9.3	-67.1	7.4	-19.1	-136.7	16.2
2016-08-19	Rain	31.7	62	5.7	8.0	-6.1	-43.2	5.6	-17.2	-122.0	16.0
2016-08-25	Rain	23.1	88	38.1	17.0	-5.7	-34.2	11.4			
2016-08-26	Rain	22.2	64	0.9	10.0	4.7	11.3	-26.6			
2016-09-12	Rain	20.7	69	2.7	7.0	0.4	-5.3	-8.8	-13.8	-98.8	10.0
2016-09-13	Rain	21.1	77	0.7	1.0	-1.3	-9.6	1.0	-13.4	-93.8	13.7
2016-09-19	Rain	17.7	99	8.4	15.0	-7.5	-45.9	14.3	-16.0	-110.5	17.4
2016-09-20	Rain	18.0	99	3.8	16.0	-6.5	-42.0	9.8	-17.8	-124.0	18.0
2016-09-24	Rain	21.6	86	0.9	8.0	-3.5	-35.0	-7.3	-15.2	-111.8	9.7
2016-09-26	Rain	19.1	94	3.3	4.0	-6.3	-42.8	7.4	-15.7	-110.7	15.3
2016-10-06	Rain	14.2	98	11.3	9.0	-4.3	-20.7	13.7	-15.9	-107.1	20.4
2016-10-08	Rain	16.8	82	7.5	26.0	-4.8	-23.6	14.4	-16.5	-109.9	21.8
2016-10-09	Rain	13.5	86	6.3	7.0	-6.5	-43.2	9.1	-16.1	-108.5	20.4
2016-10-12	Rain	14.1	99	0.3	1.0	-3.3	-20.9	5.9	-15.5	-104.0	20.0
2016-10-14	Rain	15.0	80	3.3	7.0	-3.2	-33.7	-8.4	-17.7	-123.6	17.7
2016-10-15	Rain	13.6	98	1.5	4.0	-8.0	-54.6	9.1	-18.9	-131.7	19.3
2016-10-21	Rain	17.1	91	7.1	12.0	-9.1	-65.3	7.6			
2016-10-22	Rain	13.2	97	7.0	13.0	-6.6	-32.3	20.7			
2016-10-23	Rain	11.7	99	2.7	11.0	-9.0	-50.8	21.0			
2016-10-24	Rain	10.0	97	9.5	8.0	-14.3	-98.3	15.7			
2016-10-25	Rain	9.8	99	2.3	3.0	-13.0	-91.3	13.1			
2016-10-26	Rain	11.0	99	4.2	21.0	-12.1	-81.8	15.4			
2016-10-27	Rain	10.6	94	6.9	17.0	-11.1	-73.6	15.6			
2016-11-06	Rain	11.0	97	0.8	2.0	-6.7	-35.5	18.2	-16.7	-114.7	18.7
2016-11-07	Rain	10.0	80	0.7	3.0	-6.1	-27.1	22.0	-19.1	-129.4	23.0
2016-11-22	Snow	-1.1	85	4.4	21.0	-12.3	-76.7	21.9	-18.7	-124.5	25.4
2016-12-03	Rain	7.0	80	0.5	11.0	-5.8	-34.0	12.2	-18.2	-126.3	18.9
2016-12-21	Rain	4.7	77	2.1	7.0	-3.8	-13.4	17.3			
2016-12-25	Snow	2.7	70	1.1	7.0	-3.4	-17.7	9.3			

Appendix of Table S3

2017-01-06	Rain	3.0	98	1.5	29.0	-7.0	-40.0	15.7	-18.0	-129.7	14.4
2017-01-07	Rain	2.3	61	1.9	7.0	-9.6	-64.4	12.1	-21.2	-152.8	16.5
2017-02-07	Snow	2.3	82	1.3	18.0	-2.5	-10.8	9.3	-16.9	-113.0	22.2
2017-02-08	Snow	2.9	58	1.1	8.0	-3.8	-24.8	5.6	-21.7	-155.7	17.9
2017-02-21	Snow	1.2	77	3.7	12.0	-9.0	-68.2	3.7	-15.0	-96.6	23.6
2017-03-13	Rain	3.0	99	27.0	10.0	-9.9	-60.6	18.4			
2017-03-15	Rain	4.9	87	0.5	9.0	-2.3	-9.8	8.7			
2017-03-23	Rain	6.8	89	0.6	5.0	0.1	17.0	16.3	-13.5	-89.6	18.7
2017-03-30	Rain	11.9	80	1.3	12.0	-2.7	-4.7	16.7	-16.9	-113.7	21.4
2017-04-03	Rain	14.6	75	0.9	5.0	1.8	5.9	-8.3	-13.8	-98.4	11.7
2017-04-08	Rain	14.9	83	1.7	6.0	-2.1	-1.6	15.0	-13.2	-87.7	18.0
2017-04-09	Rain	9.7	96	3.8	20.0	-4.2	-14.3	19.5	-15.5	-101.3	22.7
2017-04-10	Rain	7.8	95	6.0	21.0	-8.3	-49.4	17.1	-19.5	-134.5	21.2
2017-04-16	Rain	14.0	90	5.1	16.0	-2.6	-0.7	20.5	-13.5	-85.3	23.0
2017-04-19	Rain	15.7	61	0.6	5.0	0.8	-0.5	-7.1	-14.7	-100.6	17.4
2017-04-25	Rain	17.6	76	1.7	17.0	2.2	26.9	9.1			
2017-05-03	Rain	14.3	95	14.1	16.0	-5.5	-23.7	20.4	-16.2	-109.1	20.9
2017-05-14	Rain	21.4	57	0.2	6.0	8.3	55.4	-11.3	-9.0	-56.8	15.1
2017-05-15	Rain	17.5	83	6.0	6.0	-5.5	-30.2	13.6	-16.4	-114.7	16.7
2017-05-16	Rain	22.4	46	0.6	1.0	-3.1	-23.1	2.0	-17.3	-125.2	13.1
2017-05-22	Rain	19.3	83	8.3	8.0	-3.3	-9.3	17.3	-16.0	-105.4	22.6
2017-05-23	Rain	19.0	62	0.6	1.0	-3.3	-20.1	6.2	-18.0	-125.8	18.0
2017-05-29	Rain	23.1	62	0.6	4.0	4.1	33.3	0.3	-8.0	-48.0	15.9
2017-06-03	Rain	24.0	65	2.0	3.0	3.3	28.7	2.0	-8.9	-55.3	16.3
2017-06-04	Rain	15.9	99	12.4	8.0	-0.2	10.9	12.1	-10.5	-68.8	15.6
2017-06-05	Rain	15.8	99	7.9	16.0	-5.6	-31.4	13.7	-15.7	-109.6	16.1
2017-06-08	Rain	22.3	80	0.6	13.0	-2.6	-12.0	9.0	-14.7	-100.0	17.9
2017-06-09	Rain	21.4	98	0.5	8.0	0.2	0.4	-1.5	-14.0	-94.4	17.9
2017-06-10	Rain	22.4	75	2.2	6.0	-3.9	-19.1	12.4	-14.7	-98.8	19.1
2017-06-29	Rain	27.8	54	0.3	4.0	0.2	-1.9	-3.7	-13.7	-93.9	16.6
2017-07-05	Rain	27.3	66	0.3	2.0	-3.8	-41.3	-10.6			
2017-07-06	Rain	23.5	85	10.8	20.0	-9.2	-66.9	6.7			
2017-07-16	Rain	27.7	67	1.1	1.0	-6.6	-54.2	-1.6	-17.8	-127.1	15.1
2017-07-27	Rain	32.3	61	7.9	0.5	-10.5	-74.3	10.0	-20.3	-143.8	18.8
2017-07-28	Rain	23.7	96	5.7	2.0	-8.8	-67.3	3.0	-19.9	-139.3	19.6
2017-07-30	Rain	25.3	76	3.1	6.0	-7.5	-54.2	5.6	-18.5	-130.1	18.2
2017-08-13	Rain	25.8	76	5.1	3.0	-7.2	-48.5	9.2	-18.2	-128.4	16.9
2017-08-14	Rain	25.6	81	3.2	5.0	-7.4	-52.5	6.9	-18.2	-127.6	17.8
2017-08-21	Rain	28.0	78	0.8	1.0	-6.1	-46.0	2.7			
2017-08-25	Rain	22.6	70	1.1	17.0	1.0	2.3	-6.0			
2017-08-26	Rain	19.6	96	0.2	5.0	-2.0	-5.8	10.2			
2017-08-28	Rain	20.0	90	2.1	9.0	-10.9	-75.2	11.6			
2017-08-29	Rain	17.3	99	7.0	24.0	-10.7	-72.1	13.4			
2017-08-30	Rain	16.0	99	5.4	25.0	-11.4	-76.1	15.1			
2017-09-02	Rain	21.1	91	3.1	10.0	-13.9	-103.8	7.2			
2017-09-03	Rain	18.8	95	2.1	5.0	-12.9	-95.2	7.7			
2017-09-04	Rain	18.3	99	1.3	5.0	-11.2	-82.9	6.9			
2017-09-05	Rain	18.0	99	4.8	16.0	-15.7	-115.0	10.3			
2017-09-09	Rain	19.8	99	11.1	27.0	-12.7	-90.5	11.0			
2017-09-16	Rain	19.4	96	13.4	11.0	-5.9	-34.8	12.7			
2017-09-19	Rain	19.4	96	8.6	8.0	-6.1	-35.0	13.9			
2017-09-19	Rain	23.5	75	0.3	1.0	-2.8	-25.3	-3.2	-15.1	-106.4	14.3
2017-09-25	Rain	19.9	87	2.9	11.0	-9.1	-64.9	7.5	-18.4	-133.9	13.3
2017-09-26	Rain	18.0	82	7.0	24.0	-12.7	-90.1	11.6	-19.5	-135.5	20.3
2017-09-27	Rain	16.3	98	20.2	16.0	-9.8	-59.7	18.8	-19.9	-137.2	22.1
2017-10-01	Rain	18.0	95	3.2	12.0	-6.7	-41.2	12.2	-16.7	-118.3	15.1
2017-10-02	Rain	18.0	92	1.9	2.0	-7.5	-47.2	12.7	-17.8	-124.1	18.0
2017-10-03	Rain	12.4	98	13.3	9.0	-9.3	-53.0	21.6	-23.5	-165.4	22.6
2017-10-04	Rain	11.0	96	15.6	16.0	-18.2	-131.7	14.2	-27.8	-201.4	20.7
2017-10-08	Rain	16.1	97	0.6	10.0	-11.3	-79.4	11.3	-21.4	-153.7	17.5
2017-10-09	Rain	12.6	87	0.3	5.0	-9.3	-62.4	12.4			
2017-10-10	Rain	8.1	93	6.0	12.0	-13.3	-91.0	15.0			
2017-10-11	Rain	7.1	98	14.6	7.0	-17.0	-119.8	15.9			
2017-10-12	Rain	11.5	86	4.8	13.0	-17.6	-127.5	13.2			
2017-10-15	Rain	11.8	97	3.7	12.0	-13.9	-99.1	11.9	-22.6	-162.3	18.5
2017-10-16	Rain	11.5	97	0.3	12.0	-10.9	-69.9	17.5	-20.3	-144.5	17.7
2017-10-25	Rain	13.5	93	0.3	5.0	-3.9	-33.9	-2.8			
2017-10-30	Rain	10.5	79	0.3	2.0	-2.4	-18.3	0.6			
2017-11-01	Rain	11.1	96	1.2	10.0	-7.1	-37.6	19.3			
2017-11-10	Rain	9.7	72	3.0	4.0	-5.8	-25.5	21.2			

References

- Araguás-Araguás, L., Froehlich, K. and Rozanski, K.: Deuterium and oxygen-18 isotope composition of precipitation and atmospheric moisture, *Hydrol. Process.*, 14(8), 1341–1355, doi:10.1002/1099-1085(20000615)14:8<1341::AID-HYP983>3.3.CO;2-Q, 2000.
- Barnes, S. L.: An Empirical Shortcut to the Calculation of Temperature and Pressure at the Lifted Condensation Level, *J. Appl. Meteorol. Climatol.*, 7(3), 511, doi:10.1175/1520-0450(1968)007<0511:AESTTC>2.0.CO;2, 1968.
- Benetti, M., Reverdin, G., Pierre, C., Merlivat, L., Risi, C., Steen-Larsen, H. C. and Vimeux, F.: Deuterium excess in marine water vapor: Dependency on relative humidity and surface wind speed during evaporation, *J. Geophys. Res.*, 119(2), 584–593, doi:10.1002/2013JD020535, 2014.
- Best, A. C.: Empirical formulae for the terminal velocity of water drops falling through the atmosphere, *Q. J. R. Meteorol. Soc.*, 76(329), 302–311, doi:10.1002/qj.49707632905, 1950a.
- Best, A. C.: The size distribution of raindrops, *Q. J. R. Meteorol. Soc.*, 76(327), 16–36, doi:10.1002/qj.49707632704, 1950b.
- Deshpande, R. D., Maurya, A. S., Kumar, B., Sarkar, A. and Gupta, S. K.: Rain-vapor interaction and vapor source identification using stable isotopes from semiarid western India, *J. Geophys. Res. Atmos.*, 115(23), 1–11, doi:10.1029/2010JD014458, 2010.
- Ellehoj, M. D., Steen-Larsen, H. C., Johnsen, S. J. and Madsen, M. B.: Ice-vapor equilibrium fractionation factor of hydrogen and oxygen isotopes: experimental investigations and implications for stable water isotope studies, *Rapid Commun. Mass Spectrom. Rcm*, 27(19), 2149–2158, 2013.
- Górnicki, K., Winiczenko, R., Kaleta, A. and Choińska, A.: Evaluation of models for the dew point temperature determination, *Tech. Sci.*, 20(3 SE-Artykuły), 241–257, doi:10.31648/ts.5425, 2017.
- von Herrmann, C. F.: Problems in meteorology, *Mon. Wea. Rev.*, 34, 574–579, doi:10.1175/1520-0493(1906)34,574:PIM.2.0.CO;2, 1906.
- Horita, J. and Wesolowski, D. J.: Liquid-vapor fractionation of oxygen and hydrogen isotopes of water from the freezing to the critical temperature, *Geochim. Cosmochim. Acta*, 58(16), 3425–3437, 1994.
- Kinzer, G. D. and Gunn, R.: THE EVAPORATION, TEMPERATURE AND THERMAL RELAXATION-TIME OF FREELY FALLING WATERDROPS, *J. Meteorol.*, 8(2), 71–83, doi:10.1175/1520-0469(1951)008<0071:TETATR>2.0.CO;2, 1951.
- Noone, D., Risi, C., Bailey, A., Berkelhammer, M., Brown, D. P., Buenning, N., Gregory, S., Nusbaumer, J., Schneider, D., Sykes, J., Vanderwende, B., Wong, J., Meillier, Y. and Wolfe, D.: Determining water sources in the boundary layer from tall tower profiles of water vapor and surface water isotope ratios after a snowstorm in Colorado, *Atmos. Chem. Phys.*, 13(3), 1607–1623, doi:10.5194/acp-13-1607-2013, 2013.
- Parameswaran, K. and Murthy, B. V. K.: Altitude Profiles of Tropospheric Water Vapor at Low Latitudes, *J. Appl. Meteorol.*, 29(8), 665–679, doi:10.1175/1520-0450(1990)029<0665:APOTWV>2.0.CO;2, 1990.
- Sonntag, C., Rozanski, K., Munnich, K. and Jacob, H.: Variations of deuterium and oxygen-18 in continental precipitation and groundwater and their causes, in In Variations in the Global Water Budget, edited by S.-P. A, pp. 107–124, D. Reidel Publishing Company, Dordrecht., 1983.
- Stewart, M. K.: Stable isotope fractionation due to evaporation and isotopic exchange of falling waterdrops: Applications to atmospheric processes and evaporation of lakes, *J. Geophys. Res.*, 80(9), 1133–1146, doi:10.1029/JC080i009p01133, 1975.

Wang, S., Zhang, M., Che, Y., Zhu, X. and Liu, X.: Influence of Below-Cloud Evaporation on Deuterium Excess in Precipitation of Arid Central Asia and Its Meteorological Controls, *J. Hydrometeorol.*, 17(7), 1973–1984, doi:10.1175/JHM-D-15-0203.1, 2016.

Weng, Y., Touzeau, A. and Sodemann, H.: Correcting the impact of the isotope composition on the mixing ratio dependency of water vapour isotope measurements with cavity ring-down spectrometers, *Atmos. Meas. Tech.*, 13(6), 3167–3190, doi:10.5194/amt-13-3167-2020, 2020.

Wu, H., Fu, C., Zhang, C., Zhang, J., Wei, Z. and Zhang, X.: Temporal Variations of Stable Isotopes in Precipitation from Yungui Plateau: Insights from Moisture Source and Rainout Effect, *J. Hydrometeorol.*, 23(1), 39–51, doi:10.1175/JHM-D-21-0098.1, 2022.